Research Article

Mechanical Properties of Municipal Solid Waste Incinerator (MSWI) Bottom Ash as Alternatives of Subgrade Materials

Yucheng Huang,[1,2] Ji Chen,[1] Shenjie Shi,[1] Bin Li,[1] Jialin Mo,[1,3,4] and Qiang Tang[1,3,5]

[1]*School of Rail Transportation, Soochow University, Xiangcheng District, Suzhou 215131, China*
[2]*Virginia Polytechnic Institute and State University, Blacksburg, VA 24061, USA*
[3]*Graduate School of Global Environmental Studies, Kyoto University, Sakyo-Ku, Kyoto 606-8501, Japan*
[4]*National Institute for Environmental Studies, Fukushima Branch, Fukushima 963-7700, Japan*
[5]*National Engineering Laboratory of Highway Maintenance Technology, Changsha University of Science & Technology, Changsha 410114, Hunan, China*

Correspondence should be addressed to Qiang Tang; tangqiang@suda.edu.cn

Received 7 December 2019; Accepted 9 January 2020; Published 30 January 2020

Academic Editor: Marco Corradi

The rapid development of industrialization, urbanization, and population of the society augments the rising amount of municipal solid waste (MSW). With the advantage of considerably reducing mass and volume of solid wastes and generating energy, the incineration is a widely used treatment method for MSW. During the incineration process, the organic substances contained in the wastes are combusted, and the massive residues are remained. Of the incineration residues, bottom ash takes up to 80–90%, and the remainders are fly ash along with air pollution control residues. Dealing with the municipal solid waste incineration (MSWI) bottom ash in a sustainable manner is the primary principle. Significantly, MSWI bottom ash has been successfully utilized in diverse beneficial applications in recent decades, especially in civil engineering applications. This paper investigates the mechanical properties and validity of MSWI bottom ash as applicable substitutes of conventional subgrade materials. For this reason, a series of direct shear and CBR tests are performed on specimens with different water contents and dry densities.

1. Introduction

The rapid development of industrialization, urbanization, and population of the society augments the increasing amount of municipal solid waste (MSW). The disposal of MSW has been a critical concern worldwide; meanwhile, sustainable waste management is the core principle. Landfill, compositing, recycling, and incineration are the common treatment methods for MSW [1, 2]. Due to the limit of the land resources and the potential ecological damage to the environment, incineration and recycling are preferred to landfill as the treatment method of MSW. The incineration process can reduce 70% of the mass and 90% of the volume in MSW [3], making it an appropriate treatment to dispose the large volume of waste and generate energy at the same time. The generated energy from the incineration can be used for heating and electricity system in the form of heat or steam [4]. However, the incineration treatment also brings in a large amount of incineration residues [5, 6]. Of the incineration residues, bottom ash takes up to 80–90%, and the remainder is fly ash along with air pollution control residues. Even if the advanced incineration technology is adopted, large amounts of MSWI bottom ash will also be produced, which become a critical issue due to its increasing quantity, meanwhile containing heavy metals and other hazardous pollutants. The main elements of MSWI bottom ash are Si, Al, Fe, K, Na, Ca, Mg, and Cl, whereas the oxides of these are contained [7]. For this purpose, various treatment processes are required before the recycle and reuse of bottom ash, including processes of ferrous metals removing, separation methods, thermal methods, compaction aging during storage, solidification/stabilization, verification, chemical extraction, and leaching process [8, 9].

In the past few decades, MSWI bottom ash has been successfully applied in various beneficial applications, especially in civil engineering applications. Given the great demand of construction materials, MSWI bottom ash has been widely used in road base layer, subbase layer, road subgrade, and parking lot. MSWI bottom ash, as the reuse of building materials, is conducive to reducing the production cost of raw materials, saving natural resources and solving disposal problems.

A number of researches have been carried out to further verify the beneficial reuse of MSWI bottom ash in road construction [10–14]. To some extent, MSWI bottom ash is comparable to traditional mineral aggregate, insensitive to water (from the perspective of geotechnical engineering), noncohesive, and permeable [15].

At the same time, studies have been conducted, and the results further validate the beneficial reuse of MSWI bottom ash in road constructions. MSWI bottom ash is to some extent comparable to the conventional mineral aggregates [15]. It can be utilized with the hydraulic binder as an aggregate alternative for primary sands and gravels in concrete because its particle size distribution, fine content, and compaction characteristics are comparable to the traditional aggregates [16–18]. MSWI bottom ash can also be mixed with conventional granular materials or soil at different ratios as road base/subbase or subgrade layer. The geotechnical characteristics of these mixtures such as shear strength, resilient modulus, and California bearing capacity (CBR) are comparable to those of the widely used base/subbase or subgrade materials [11, 19–26].

MSWI bottom ash is susceptible to freezing, so it is not suitable to be used as asphalt wearing course. Moreover, the MSWI bottom ash is applied in low-volume asphalt pavement in proportions and exhibits higher stiffness, greater resistance to fatigue, and rutting, whereas lower susceptibility to water compared with conventional AC 16 [13, 27].

The objective of this paper is (1) to investigate the mechanical properties of MSWI bottom ash with different densities and water content combinations and (2) to verify whether the best mechanical properties exhibit at optimum water content and maximum dry density.

2. Materials and Methods

2.1. Materials. In this paper, the MSWI bottom ash is obtained from Qizishan Waste Incineration Plant in Wuzhong district, Suzhou, China. The MSWI bottom ash is commonly crushed into smaller particle sizes and desired gradation for recycling applications as shown in Figure 1. Approximately 6000 tons/day MSWI is generated in Suzhou, and among them, around 2500 tons is deposited and treated at this plant. The beneficial applications of MSWI residues are valuable for the sustainable development of the plant.

The particle size distribution is shown in Figure 2. It can be noted that the particle size varies in range from 0.1 to 10 mm, which is comparable to the natural aggregate size and distribution.

The C_u (coefficient of uniformity) and the C_c (coefficient of curvature) are two crude parameters to classify if the soil is well graded or not, which are calculated as following equations:

$$C_u = \frac{d_{60}}{d_{10}}, \tag{1}$$

$$C_c = \frac{d_{30}^2}{d_{60} \times d_{10}}. \tag{2}$$

The shape parameters of MSWI bottom ash are presented in Table 1, indicating they are well graded and valid as alternatives of the subgrade materials.

Figure 1: MSWI after being crushed.

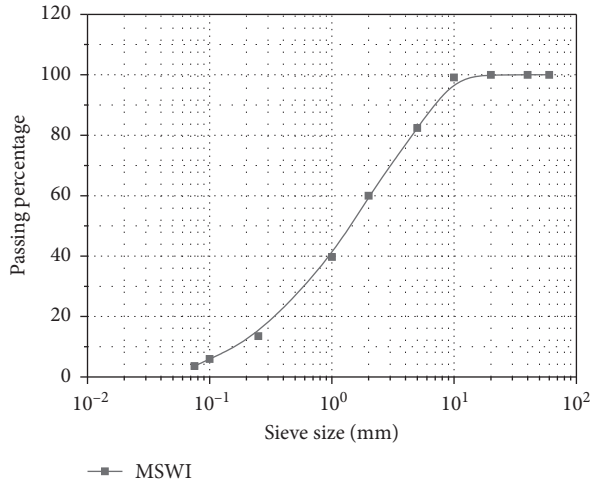

Figure 2: Gradation curve of the MSWI bottom ash.

2.2. Specimen Preparations. The MSWI bottom ash applied in this paper was dried at 105°C for 24 hours to achieve the required dry condition and then cooled to room temperature. The specimens were manufactured according to JTG E40-2007 using the hand compactor JDS-3 (Nanjing Soil Instrument, China) with the 4.5 kg hammer for the heavy duty use due to the road material application. Each specimen

Table 1: Shape parameters of MSWI.

Item	MSWI	Well-graded range
C_u	0.05	>5
C_c	44	$\in(1, 3)$

was prepared by 900 g MSWI bottom ash and compacted with three layers. During the compaction procedure, it should be ensured that each layer was compacted for 98 times as well as the height of each layer after compaction was almost the same, and the hammer height was kept at 30 cm for each compact work. It is well known that the optimum water content can be predicted based on the plastic limit. Because the plastic limit of MSWI is measured as 26.7%, the optimum water content is estimated to be around 16%. Accordingly, the six samples were manufactured with water contents of 10%, 12%, 14%, 16%, 18%, and 20%, respectively. In accordance with the compaction curve as presented in Figure 3, the maximum $\rho_d = 1.76\,\text{g/cm}^3$ and $w = 16\%$ is the optimum water content. For the following direct shear tests, a wide variety of specimens with dry density of 1.23, 1.35, 1.61, 1.68, and $1.76\,\text{g/cm}^3$ and water content of 0%, 10%, 14%, 16%, and 17.5% combinations were manufactured. The specimens for each combination had 2 replicates.

2.3. Direct Shear Test and CBR Test. The core cutter method is employed in this paper to control the dry density of the samples. Series of direct shear tests are conducted on the samples at different water contents of 0%, 10%, and 16% with the same ρ_d of $1.23\,\text{g/cm}^3$, following tests at different ρ_d of 1.23, 1.35, and $1.61\,\text{g/cm}^3$ with the same water content of 10%. All the aforementioned series of tests are performed at different vertical stresses of 50, 100, 200, 300, and 400 kPa. The purpose of these tests is to evaluate the effects of water content, dry density, and vertical stress on the shear strength of MSWI.

CBR (California bearing ratio) is a method of classifying and evaluating materials for flexible pavements [7], which is used to evaluate the penetration resistance of the material to the standard plunger under controlled moisture and density. In this paper, the CBR tests are conducted for specimens with 5 water contents of 10%, 14%, 16%, 18%, and 20%.

2.4. Finite Element Modeling of Pavements with MSWI Bottom Ash. The finite element model of common pavement structure is established, and the response and performance of pavement structure with and without MSWI bottom ash are evaluated. The commercial finite element software ABAQUS is used for simulation. As shown in Figure 4, the pavement consists of 15 cm hot mix asphalt (HMA), 25 cm unbonded granular base, and 1.5 m subgrade. It is difficult and time consuming to determine the modulus of resilience with triaxial shear test equipment. For this purpose, the modulus of elasticity is estimated according to the CBR value. The conversion between the modulus of elasticity and the CBR value of MSWI bottom ash is described in accordance with the Asphalt Institute's soil manual for the

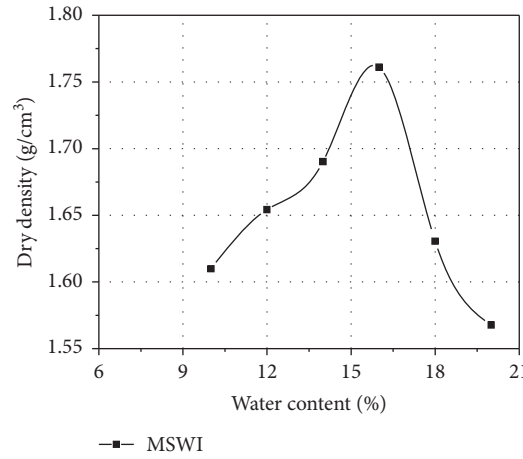

Figure 3: Compaction curves for MSWI.

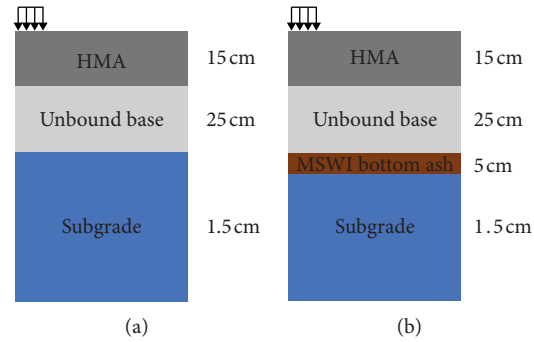

Figure 4: Pavement structure in the finite element model.

design of asphalt pavement structures [28]. The conversion formula is as follows:

$$\text{Mr (Mpa)} = 10.342\,\text{CBR}. \quad (3)$$

Aiming to simulate the pavement dynamic response in a more realistic manner, the 3-dimensional pavement structure model subjected to the moving tire load is employed in this paper, as shown in Figure 5. At the initial step, the tire print load is applied on #1 to #6 elements, then the load is removed on element #1 and imposed on the element #7, step by step until the imprint passes through the loading area as one load cycle (Figure 6). It is noted that the typical simplification for repeated moving tire load is to use cyclic plate loads [29], in which the cyclic load time is equivalent to the load duration (time of passing the imprint at certain speed multiplied by the load cycles). However, according to the previous study, compared with moving load with equivalent load magnitude and number of cycles, much lower permanent deformations are observed in the cyclic plate loads due to the shear stress reversal [30, 31]. It is resulting from the direction principal stresses rotate and shear stress reversals (tension to compression or vice versa). Consequently, although more time consuming, the moving load simulation is closer to the wheel load mechanism, than the cyclic plate load method.

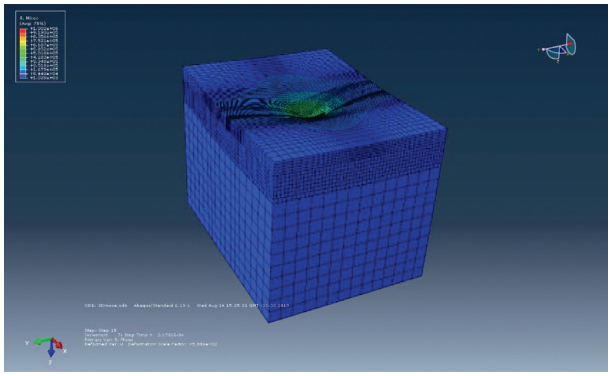

Figure 5: 3-Dimensional pavement model subjected to moving load.

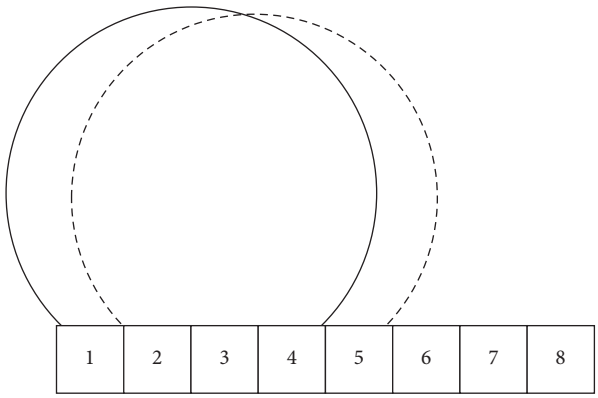

Figure 6: Loading step of moving load.

3. Results and Discussions

3.1. Direct Shear Test Results. The shear test results are presented as below in Figure 7 for specimens at different water contents of 0%, 10%, and 16% and various vertical pressures of 50, 100, 200, 300, and 400 kPa, while with the same dry density of 1.23 g/cm^3. It can be noted that the shear stress tends to increase with the rising of the shear displacement, and the profound differences of shear stress among different water contents exhibit at the low vertical stress. Meanwhile, with the increase of vertical pressure, the differences among the different water contents decrease and no significant differences are observed. The test results are summarized in Table 2, implying with the same water content, the shear stress goes up with the vertical stress increasing. As can be seen, no peak point is observed in Figure 7, which probably results from the low density of 1.23 g/cm^3. Different direct shear tests were studied to evaluate the shear strength, as well as the cohesion and friction angle [19, 32–34]. The results show that the strength and friction angle of dry bottom ash and saturated bottom ash are 34.8°~51.1° and 26.0°~37.2°, respectively. The deformation decreases with the increase of shear stress, and the strength and stiffness decrease with the increase of wet stress. The results of this paper are similar to those mentioned above.

Different shear tests are carried out on specimens of different dry densities with the same water content of 10%. In Figure 8, the maximum shear stress is observed for specimens with $\rho_d = 1.61$ g/cm^3, while shear stress continuously increases with shear displacement, and no peak point is occurred for specimens with low density of 1.23 g/cm^3 and 1.35 g/cm^3. Meng used direct shear test to study the variation of shear stress with shear displacement. Under different normal stresses, the strength of the saturated specimen is lower than that of the dry specimen, indicating that the higher the water content is, the lower the shear strength is. In addition, the stiffness of saturated specimen is also smaller than that of the dry specimen, which indicates that the increase of water content may lead to the decrease of stiffness and strength. The curve in Meng's study is similar to that in this paper. In the early stage, the initial shear stress increases with the increase of shear displacement. When the stress is close to the failure state, the peak strength is not obvious. Except for the specimens with $\rho_d = 1.61$ g/cm^3, all specimens show fairly tough behavior. The above behavior was also observed in other density samples [35].

Because no peak values are observed in Figures 7 and 8, the supplementary experiments are also performed for specimens with different water content and dry density. The peak shear stresses occur at all the curves in Figure 9. It is observed that shear stress increases proportionally with shear displacement at the early stage, following a slower approach to a peak value, and then decreases to a stable value. It is noted that the higher shear stresses exhibit at greater vertical pressures which is due to the larger interlock and friction among the particles with the greater vertical pressures. The specimens with $\omega = 16\%$, $\rho_d = 1.76$ g/cm^3 present the greatest shear stress and dilatancy compared with the specimens with different water contents and dry densities. According to previous studies [26, 36–38], and compared with previous studies, the maximum dry density ($\rho_d = 1.76$ g/cm^3) and optimum water content ($\omega = 16\%$) in this paper are reasonable.

Based on the test results presented in Table 3, the relationship between shear strength and vertical stress is obtained, and then the Mohr—Coulomb equation is derived. Accordingly, the internal friction angle φ and cohesion C are calculated as shown in Table 4. In previous studies, the friction angle is from 25° to 50°. The cohesion measured by the triaxial test of consolidated drainage is between 13.8 and 34.5 kPa [39–42]. The frictional angle of bottom ash varies greatly. Influenced by complex factors, the frictional angle and cohesion of this paper are relatively low, mainly because the water content used in previous studies is 20% and nearly 5% higher than that used in this paper.

Song studied the influence of water contents on the strength properties of MSWI bottom ash. The results show that the best water content is about 15.5% with the largest dry density of about 1.52 g·cm^{-3}, which are for well-graded gravel soils and close to the results of this paper. The mechanical mechanism is that the cohesion increases with the increase of water content in the range of optimum water content. When the optimum water content reaches, the cohesion and internal friction angle decreases, and the shear strength increases. The water content shows significant

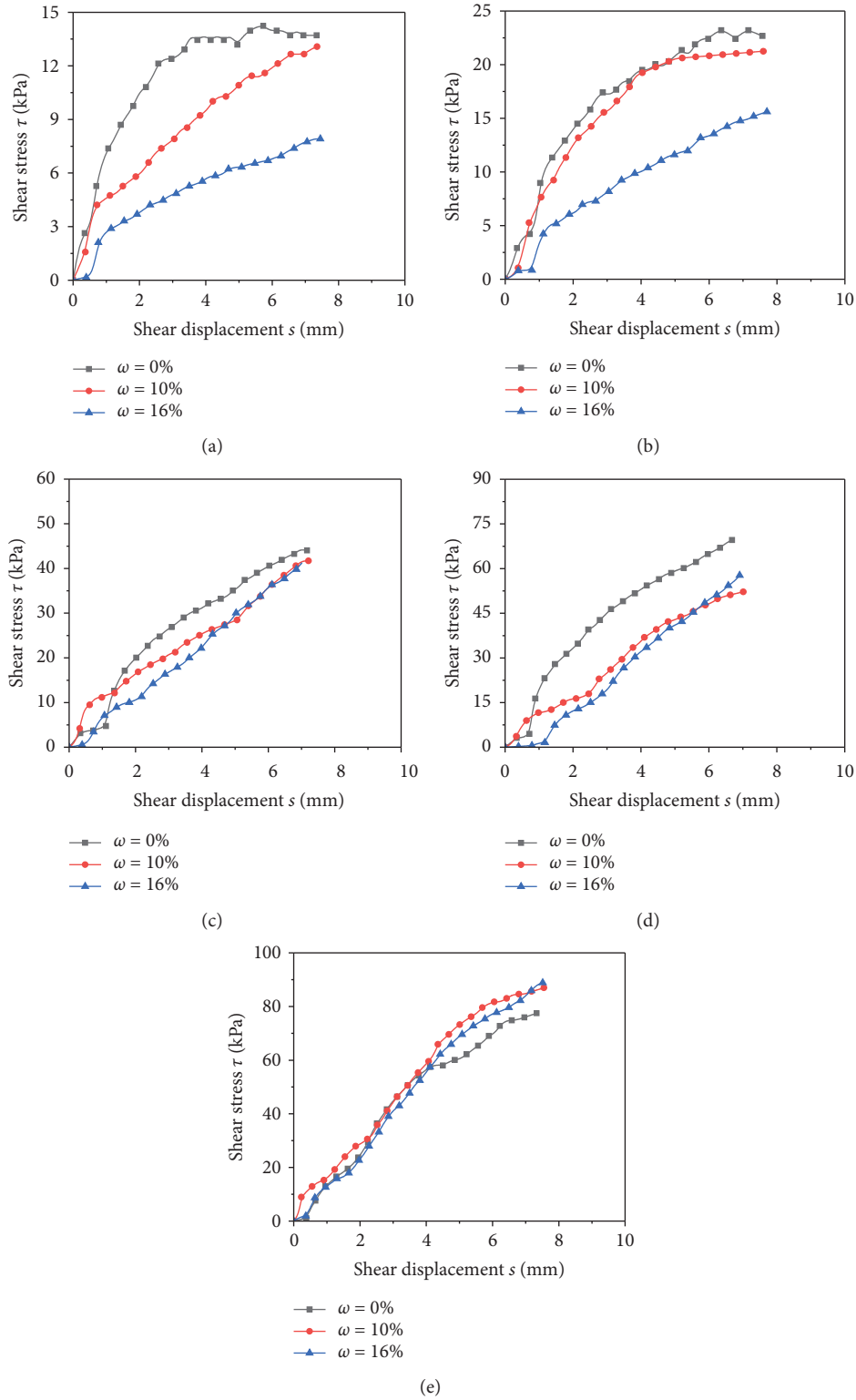

FIGURE 7: Shear stress versus shear displacement with different water contents. (a) Vertical pressure 50 kPa, (b) vertical pressure 100 kPa, (c) vertical pressure 200 kPa, (d) vertical pressure 300 kPa, and (e) vertical pressure 400 kPa.

influence on the strength [43]. Based on the test results, the same as the conventional natural aggregates, the maximum shear strength and dilatancy of MSWI bottom ash are observed at maximum dry density and optimum water content. Owing to the characteristic similarities between MSWI bottom ash and natural aggregates, it is recommended that the MSWI bottom ash is compacted for applications as road subgrade or base materials [44].

Table 2: Shear strength of specimens at density of 1.23 g/cm^3.

Vertical stress (kPa)	Shear strength (kPa)		
	Water content 0%	Water content 10%	Water content 16%
50	13.71	9.49	5.8
100	19.51	15.25	13.02
200	31.11	23.47	20.15
300	43.68	36.91	32.17
400	55.90	50.60	43.63

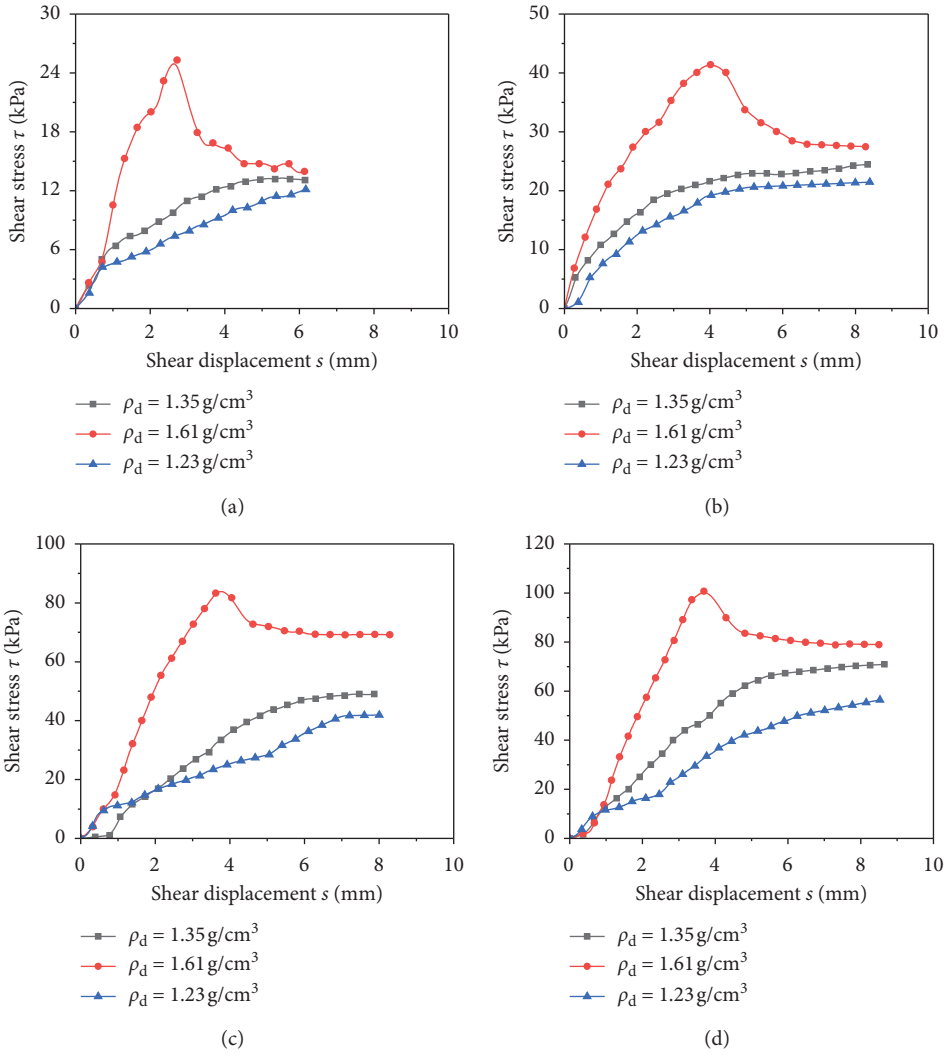

Figure 8: Continued.

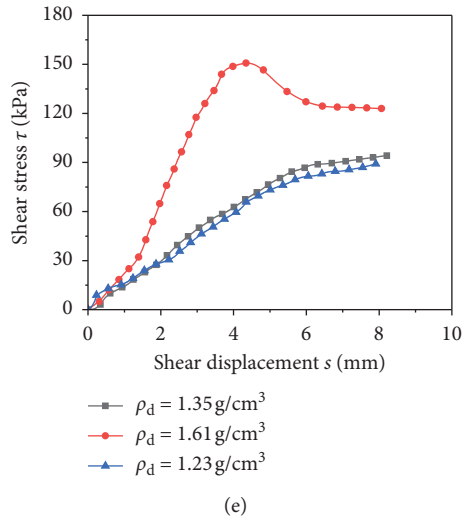

FIGURE 8: Shear stress versus shear displacement with different dry densities. (a) Vertical pressure 50 kPa, (b) vertical pressure 100 kPa, (c) vertical pressure 200 kPa, (d) vertical pressure 300 kPa, and (e) vertical pressure 400 kPa.

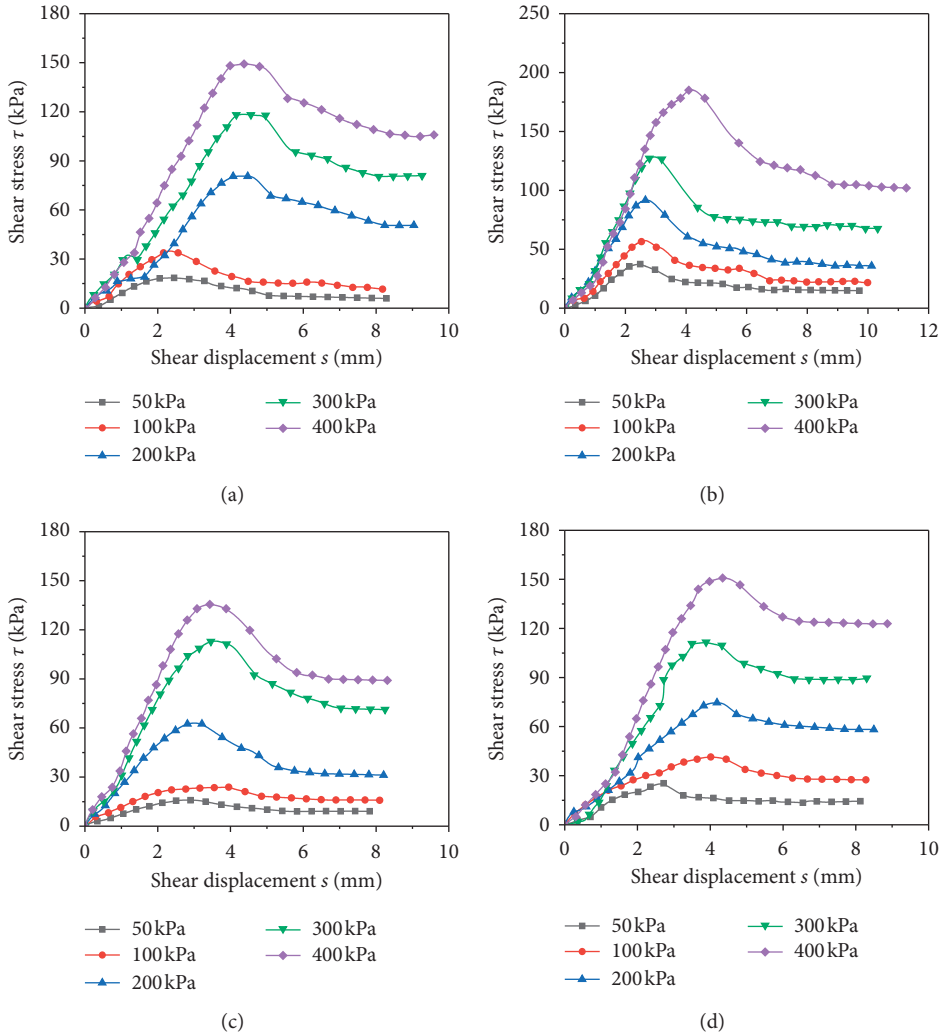

FIGURE 9: Supplementary shear stress versus shear displacement with different water contents and dry densities. (a) Water content $\omega = 17.5\%$, $\rho_d = 1.68\ g/cm^3$, (b) water content $\omega = 16\%$, $\rho_d = 1.76\ g/cm^3$, (c) water content $\omega = 14\%$, $\rho_d = 1.68\ g/cm^3$, and (d) water content $\omega = 10\%$, $\rho_d = 1.61\ g/cm^3$.

Table 3: Test results summary.

	Vertical stress (kPa)	Shear stress (kPa)	Residual stress (kPa)	Peak residuals (kPa)	Dilatancy (mm)
$\omega = 10\%$ $\rho_d = 1.61$ g/cm^3	50	25.3	14.4	10.9	0.86
	100	41.4	27.5	13.9	0.78
	200	74.4	58.2	16.2	0.54
	300	110.7	89.5	21.2	0.24
	400	148.7	122.9	25.8	0.09
$\omega = 14\%$, $\rho_d = 1.68$ g/cm^3	50	14.2	9.1	5.1	1.49
	100	23.8	15.8	8	0.84
	200	62.5	31.2	31.3	0.81
	300	113.4	71.2	42.2	0.8
	400	135.5	89.1	46.4	0.66
$\omega = 16\%$, $\rho_d = 1.76$ g/cm^3	50	37.4	14.9	22.5	2.03
	100	58.5	21.6	36.9	1.28
	200	91.8	35.9	55.9	1.04
	300	129.2	67.5	61.7	0.91
	400	181.9	102	79.9	0.83
$\omega = 17.5\%$, $\rho_d = 1.68$ g/cm^3	50	18.19	5.91	12.28	1.31
	100	35.33	11.6	23.73	0.96
	200	80.53	50.54	29.99	0.5
	300	114.96	80.95	34.01	0.46
	400	148.2	106.6	41.6	0.44

Table 4: Internal friction angles and cohesions corresponding to different conditions.

Water content (%)	Dry density (g/cm^3)	Internal friction angle φ (°)	Cohesion (kPa)
0.0	1.23	6.90	7.43
10.0	1.23	6.60	2.80
16.0	1.23	6.00	0.87
10.0	1.35	7.80	7.49
10.0	1.61	19.40	6.16
14.0	1.68	18.80	0.43
17.5	1.68	20.70	0.30
16.0	1.76	21.80	15.7

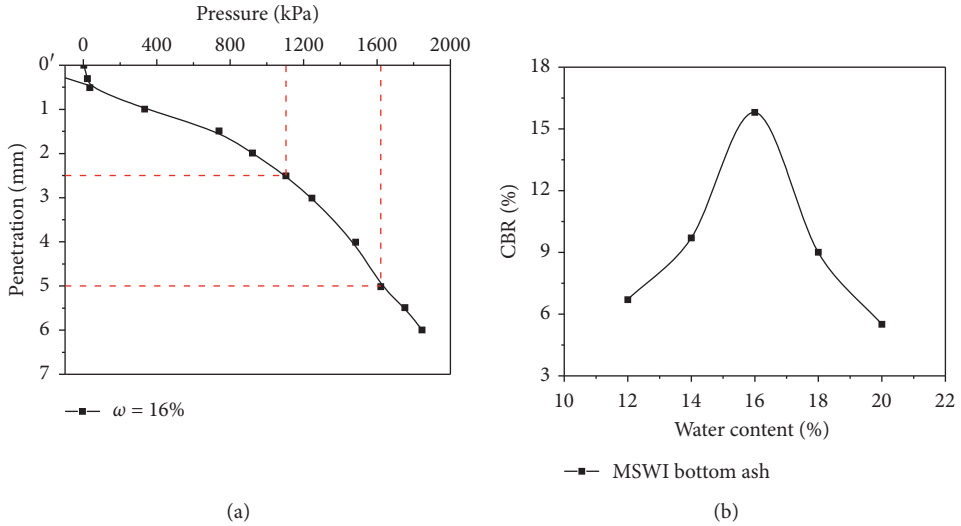

Figure 10: Penetration at water content of 16% and CBR at different water contents.

3.2. CBR Test Results. Figure 10 shows the penetration versus pressure at the water content of 16% and the CBRs at different water contents. It is worth noting that CBR is the largest when the optimum water content is 16%. Audrius conducted an experimental study on the application of MSWI as a building material in the pavement structure layer. The results of CBR test show that with the change of water content, the CBR value increases first and then decreases.

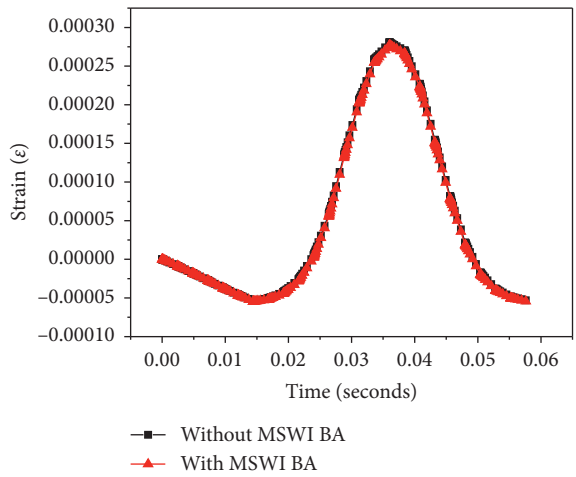

Figure 11: Strain at underside of HMA layer.

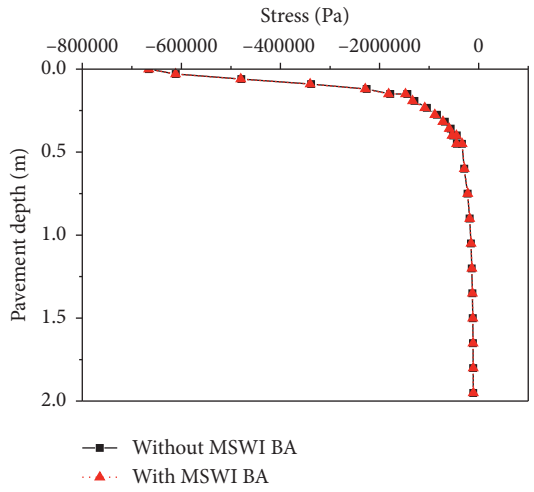

Figure 12: Compressive stress along the pavement depth.

Under the optimum water content of 16.6%, the CBR value is the largest [45]. R. Forteza studied the effects of MSWI components on engineering properties and CBR tests on cases of different densities. The experimental results show that the use of bottom ash seems to be feasible in actual pavement of road bases [26, 46–48]. In light of the road subgrade design specification JTG D30-2015, the CBR of MSWI bottom ash satisfies the requirements of CBR values as subgrade materials.

3.3. Finite Element Analysis. The strain history at the underside of the HMA layer in the model with/without MSWI bottom ash is depicted as Figure 11. At the same time, Figure 12 presents the compressive stress distribution along the pavement depth. As shown in Figures 11 and 12, although the presence of MSWI bottom ash slightly reduces the strain at the bottom of the HMA and the compressive stress along the depth, the stress and strain values are comparable in both models. The results show that the tensile strain diminishes at the bottom of HMA and the compressive strain decreases at the top of subgrade, thus reducing fatigue and rutting damage.

4. Conclusions

To research the mechanical properties of MSW incineration bottom ash as subgrade material, and observe its best performance under the optimum water content and maximum dry density, CBR test and a series of direct shear test were carried out on the samples with different water content and dry density. To further verify the feasibility of MSWI as a subgrade alternative, a three-dimensional finite element model of pavement is established, and the response of pavement under moving load in the model is compared. The following conclusions are drawn:

(1) The MSWI bottom ash after being crushed from Qizishan Waste Incineration Plant are comparable to the traditional aggregates in terms of particle size distribution, fines content, and compaction characteristics.

(2) The C_u and the C_c of MSWI bottom are both in the well-graded range, indicating it has reasonable size distribution and validity as alternatives of the subgrade materials.

(3) The maximum shear strength and dilatancy of MSWI bottom ash are observed at the optimum water content $\omega = 16\%$ and maximum dry density $\rho_d = 1.76\ \text{g/cm}^3$, which are the same as conventional natural aggregates. It is recommended that the MSWI bottom ash is compacted for applications as road subgrade or base materials.

(3) 4. It is seen that placing a MSWI bottom ash layer between unbound base course and subgrade diminishes the tensile strain at the bottom of HMA, and lessens compressive strains on top of subgrade, indicating it can mitigate the fatigue and rutting damage. It is concluded that the presence of MSWI bottom ash layer between unbound base course and subgrade is beneficial to prolong the service life and reduce the rutting distress of asphalt pavements.

Data Availability

I declare that all the data presented in the manuscript were obtained from laboratory tests at Soochow University in Suzhou China. All the laboratory testing data were presented in the figures and tables in the manuscript. We will be very pleased to share all the raw data. If needed, please contact us via corresponding author's e-mail.

Conflicts of Interest

The authors declare that they have no conflicts of interest.

Acknowledgments

This study was supported by the National Natural Science Foundation of China (51778386, 51708377, 51608059),

Natural Science Foundation of Jiangsu Province (BK20170339), Natural Science Fund for Colleges and Universities in Jiangsu Province (17KJB560008), Open Fund of National Engineering Laboratory of Highway Maintenance Technology (Changsha University of Science and Technology) (kfj180105), and a project from Jiangsu Provincial Department of Housing, Urban-Rural Development (2016ZD18 and 2017ZD002).

References

[1] Y. Zhang, T. Ma, M. Ling, and X. Huang, "Mechanistic sieve size classification of aggregate gradation by characterizing load carrying capacity of inner structures," *Journal of Engineering Mechanics*, vol. 145, no. 9, Article ID 04019069, 2019.

[2] Q. Tang, T. Katsumi, T. Inui, and Z. Li, "Membrane behavior of bentonite-amended compacted clay," *Soils and Foundations*, vol. 54, no. 3, pp. 329–344, 2014.

[3] Q. Tang, H. J. Kim, K. Endo, T. Katsumi, and T. Inui, "Size effect on lysimeter test evaluating the properties of construction and demolition waste leachate," *Soils and Foundations*, vol. 55, no. 4, pp. 720–736, 2015.

[4] Q. Tang, Y. Liu, F. Gu, and T. Zhou, "Solidification/stabilization of fly ash from a municipal solid waste incineration facility using Portland cement," *Advances in Materials Science and Engineering*, vol. 2016, Article ID 7101243, 10 pages, 2016.

[5] Confederation of European Waste-to-Energy Plants (CEWEP), 2013, http://www.cewep.eu/information/data/graphs/m_1415.

[6] Ministry of the Environment of Japan, *The Outline of Waste treatment in Japan: Results of Fiscal Year*, in Japanese, 2013.

[7] Q. Tang, F. Gu, Y. Zhang, Y. Zhang, and J. Mo, "Impact of biological clogging on the barrier performance of landfill liners," *Journal of Environmental Management*, vol. 222, pp. 44–53, 2018.

[8] Q. Tang, F. Gu, Y. F. Gao, T. Inui, and T. Katsumi, "Desorption characteristics of Cr(III), Mn(II) and Ni(II) in contaminated soil using citric acid and citric acid containing wastewater," *Soils and Foundations*, vol. 58, no. 1, pp. 50–64, 2018.

[9] Q. Tang, F. Gu, H. Chen, C. Lu, and Y. Zhang, "Mechanical evaluation of bottom ash from municipal solid waste incineration used in roadbase," *Advances in Civil Engineering*, vol. 2018, Article ID 5694908, 8 pages, 2018.

[10] J. Zhang, J. Peng, W. Liu, and W. Lu, "Predicting resilient modulus of fine-grained subgrade soils considering relative compaction and matric suction," *Road Materials and Pavement Design*, 2019.

[11] J. Zhang, J. Peng, L. Zeng, J. Li, and F. Li, "Rapid estimation of resilient modulus of subgrade soils using performance-related soil properties," *International Journal of Pavement Engineering*, pp. 1–8, 2019.

[12] L. Zeng, L.-Y. Xiao, J.-H. Zhang, and Q.-F. Gao, "Effect of the characteristics of surface cracks on the transient saturated zones in colluvial soil slopes during rainfall," *Bulletin of Engineering Geology and the Environment*, vol. 78, no. 7, pp. 5011–5028, 2019.

[13] J. Zhang, F. Gu, and Y. Zhang, "Use of building-related construction and demolition wastes in highway embankment: laboratory and field evaluations," *Journal of Cleaner Production*, vol. 230, pp. 1051–1060, 2019.

[14] F. Gu, W. Ma, R. C. West, A. J. Taylor, and Y. Zhang, "Structural performance and sustainability assessment of cold central-plant and in-place recycled asphalt pavements: a case study," *Journal of Cleaner Production*, vol. 208, pp. 1513–1523, 2019.

[15] SETRA, LCPC, *Réalisation des remblais et des couches de forme. Guide technique*, SETRA, LCPC, Paris, France, 1992.

[16] A. Abbà, M. C. Collivignarelli, S. Sorlini, and M. Bruggi, "On the reliability of reusing bottom ash from municipal solid waste incineration as aggregate in concrete," *Composites Part B: Engineering*, vol. 58, pp. 502–509, 2014.

[17] R. Cioffi, F. Colangelo, F. Montagnaro, and L. Santoro, "Manufacture of artificial aggregate using MSWI bottom ash," *Waste Management*, vol. 31, no. 2, pp. 281–288, 2011.

[18] M. V. A. Florea, *Secondary Materials Applied in Cement-Based Products: treatment, Modelling and Environmental Interaction*, CIP-DATA Library Technische Universiteit Eindhoven, Eindhoven, Netherlands, 2014.

[19] D. Zekkos, M. Kabalan, S. M. Syal, M. Hambright, and A. Sahadewa, "Geotechnical characterization of a municipal solid waste incineration ash from a Michigan monofill," *Waste Management*, vol. 33, no. 6, pp. 1442–1450, 2013.

[20] C. J. Lynn, G. S. Ghataora, and R. K. Dhir OBE, "Municipal incinerated bottom ash (MIBA) characteristics and potential for use in road pavements," *International Journal of Pavement Research and Technology*, vol. 10, no. 2, pp. 185–201, 2017.

[21] Q. Tang, Y. Zhang, Y. Gao, and F. Gu, "Use of cement-chelated, solidified, municipal solid waste incinerator (MSWI) fly ash for pavement material: mechanical and environmental evaluations," *Canadian Geotechnical Journal*, vol. 54, no. 11, pp. 1553–1566, 2017.

[22] F. Gu, H. Sahin, X. Luo, R. Luo, and R. Lytton, "Estimation of resilient modulus of unbound aggregates using performance-related base course properties," *Journal of Materials in Civil Engineering*, vol. 27, no. 6, Article ID 04014188, 2015.

[23] F. Gu, Y. Zhang, C. Droddy, R. Luo, and R. Lytton, "Development of a new mechanistic empirical rutting model for unbound granular material," *Journal of Materials in Civil Engineering*, vol. 28, no. 8, Article ID 04016051, 2016.

[24] J. Zhang, J. Peng, J. Zheng, and Y. Yao, "Characterisation of stress and moisture-dependent resilient behaviour for compacted clays in south China," *Road Materials and Pavement Design*, vol. 21, no. 1, pp. 262–275, 2018.

[25] J. Zhang, J. Peng, W. Liu, and W. Lu, "Predicting resilient modulus of fine-grained subgrade soils considering relative compaction and matric suction," *Road Materials and Pavement Design*, pp. 1–13, 2019.

[26] R. Forteza, M. Far, C. Seguí, and V. Cerdá, "Characterization of bottom ash in municipal solid waste incinerators for its use in road base," *Waste Management*, vol. 24, no. 9, pp. 899–909, 2004.

[27] Y.-J. Du, N.-J. Jiang, S.-L. Shen, and F. Jin, "Experimental investigation of influence of acid rain on leaching and hydraulic characteristics of cement-based solidified/stabilized lead contaminated clay," *Journal of Hazardous Materials*, vol. 225–226, no. 10, pp. 195–201, 2012.

[28] Y. Huang, L. Wang, and H. Xiong, "Evaluation of pavement response and performance under different scales of APT facilities," *Road Materials and Pavement Design*, vol. 18, no. 3, pp. 159–169, 2017.

[29] Y. Huang, L. Wang, Y. Hou, W. Zhang, and Y. Zhang, "A prototype IOT based wireless sensor network for traffic information monitoring," *International Journal of Pavement Research and Technology*, vol. 11, no. 2, pp. 146–152. In press, 2017b.

[30] T. Ma, D. Zhang, Y. Zhang, S. Wang, and X. Huang, "Simulation of wheel tracking test for asphalt mixture using

discrete element modelling," *Road Materials & Pavement Design*, vol. 19, no. 1, pp. 1–18, 2016.

[31] Y. Huang, Y. Guan, L. Wang, J. Zhou, Z. Ge, and Y. Hou, "Characterization of mortar fracture based on three point bending test and XFEM," *International Journal of Pavement Research and Technology*, vol. 11, no. 4, pp. 339–344, 2017.

[32] C.-L. Lin, M.-C. Weng, and C.-H. Chang, "Effect of incinerator bottom-ash composition on the mechanical behavior of backfill material," *Journal of Environmental Management*, vol. 113, pp. 377–382, 2012.

[33] M.-C. Weng, C.-L. Lin, and C.-I. Ho, "Mechanical properties of incineration bottom ash: the influence of composite species," *Waste Management*, vol. 30, no. 7, pp. 1303–1309, 2010.

[34] F. Tomonori, H. Akira, D. K. Achmad, M. Norio, A. N. Huang, and K. Fukui, "Utilization of incineration fly ash from biomass power plants for zeolite synthesis from coal fly ash by microwave hydrothermal treatment," *Advanced Powder Technology*, vol. 29, no. 3, pp. 450–456, 2018.

[35] M.-C. Weng, C.-L. Lin, and C.-I. Ho, "Mechanical properties of incineration bottom ash: the influence of composite species," *Waste Management*, vol. 30, no. 7, pp. 1303–1309, 2010.

[36] B. Kim and M. Prezzi, "Compaction characteristics and corrosivity of Indiana class-F fly and bottom ash mixtures," *Construction and Building Materials*, vol. 22, pp. 672–694, 2008.

[37] M. Kamon, T. Katsumi, and Y. Sano, "MSW fly ash stabilized with coal ash for geotechnical application," *Journal of Hazardous Materials*, vol. 76, no. 2-3, pp. 265–283, 2000.

[38] I. Vegas, J. A. Ibañez, J. T. San José, and A. Urzelai, "Construction demolition wastes, Waelz slag and MSWI bottom ash: a comparative technical analysis as material for road construction," *Waste Management*, vol. 28, no. 3, pp. 565–574, 2008.

[39] J. C. Li, C. Lee, C. H. Ho, and C. J. Jeng, "Geotechnical properties of incinerator residue in taipei," in *Proceedings of the 10th Asian Regional Conference on Soil Mechanics and Foundation Engineering*, pp. 477–480, Beijing, China, 1995.

[40] W. F. Lee, Y. S. Chen, Y. Y. Chen, T. C. Hu, and D. C. Yao, "The application of combustion bottom ash in geotechnical construction," *Sino-Geotechnics*, vol. 102, pp. 69–78, 2004.

[41] D. A. Pandeline, P. J. Cosentino, E. H. Kalajian, and M. Chavez, "Shear and deformation characteristics of municipal waste combustor bottom ash for highway applications," National Research Council, 1997pp. 101–108, National Research Council, Washington, DC, USA, Transportation Research Record No. 1577, TRB.

[42] B. Muhunthan, R. Taha, and J. Said, "Geotechnical engineering properties of incinerator ash mixes," *Journal of the Air & Waste Management Association*, vol. 54, no. 8, pp. 985–991, 2004.

[43] D. Song, H. Song, G. Xiang, and X. Hong, "Influence of water contents on strength characteristics of municipal solid waste incineration bottom ash," *Journal of Hunan University*, vol. 44, no. 1, pp. 150–156, 2017.

[44] M. Izquierdo, X. Querol, A. Josa, E. Vazquez, and A. López-Soler, "Comparison between laboratory and field leachability of MSWI bottom ash as a road material," *Science of the Total Environment*, vol. 389, no. 1, pp. 10–19, 2008.

[45] A. Vaitkus, J. Gražulytė, O. Š ažul, V. Vorobjovas, and R. Kleizienė, "An algorithm for the use of MSWI bottom ash as a building material in road pavement structural layers," *Construction and Building Materials*, vol. 212, pp. 456–466, 2019.

[46] Q. Tang, P. Shi, Z. Yuan et al., "Potential of zero-valent iron in remediation of Cd (II) contaminated soil: from laboratory experiment, mechanism study to field application," *Soils and Foundations*, 2019.

[47] H. Wang, G. Wang, J. Qi et al., "Scarcity-weighted fossil fuel footprint of China at the provincial level," *Applied Energy*, vol. 258, p. 114081, 2020.

[48] H. Wang, H. Schandl, G. Wang, L. Ma, and Y. Wang, "Regional material flow accounts for China: examining China's natural resource use at the provincial and national level," *Journal of Industrial Ecology*, vol. 23, no. 6, pp. 1425–1438, 2019.